Geophysical Journal International

Geophys. J. Int. (2010) **180,** 1095–1106 doi: 10.1111/j.1365-246X.2009.04465.x

Relationships between induced polarization relaxation time and hydraulic properties of sandstone

Konstantin Titov,[1] Andrey Tarasov,[2] Yuri Ilyin,[1] Nikita Seleznev[3] and Austin Boyd[4]

[1] *St Petersburg State University, Department of Geophysics, Faculty of Geology,* 7/8 *Universitetskaya Naberezhnaya* 199034, *St Petersburg, Russia. E-mail: tito@kt4096.spb.edu*

[2] *"ElGeo" Ltd., Petrovskaya Kosa,* 1, 190000, *St Petersburg, Russia*

[3] *Schlumberger-Doll Research, One Hampshire Street, Cambridge,* MA 02139, *USA*

[4] *Schlumberger Data and Consulting Services*

Accepted 2009 November 22. Received 2009 November 6; in original form 2007 September 18

SUMMARY

We investigated electrical and physical–chemical properties of six sandstone samples with contrasting mineralogical characteristics and with hydraulic conductivity varying in a wide range. The electrical data were obtained from time domain spectral induced polarization (IP) measurements.

We inverted the IP decays to relaxation time distributions, and then compared the modal relaxation times with the dominant pore throat diameters obtained from the Mercury Injection Capillary Pressure (MICP) data.

We found a positive logarithmic relationship between the relaxation time and the pore throat diameter. Also, we found the normalized chargeability (an integral IP parameter) to be positively correlated with the clay content. These two results suggest that the polarization of our sandstones is controlled by the pore throat distribution, and by the clay content.

The logarithmic relationship contradicts previous theories, and is not universal. Adopting an approach of Kruschwitz and her co-workers, we calculated the effective diffusivity from IP and MICP data, and we found the effective diffusivity values ranging from 2.9×10^{-13} to 1.6×10^{-10} m^2 s^{-1}. High diffusivity values, typical of surface diffusion, were obtained for clean sandstones. Low diffusivity values were obtained for clayey sandstones, and they were one to two orders of magnitude lower than those characteristic of the surface diffusion.

We proposed two mechanisms to explain the 'slow' diffusion: (1) the effect of surface tortuosity of pore throats filled with clay minerals and (2) the effect of pore geometry. These two effects represent an obstacle in assessing the pore throat diameter and hydraulic conductivity of sandstones with large specific surface and clay content on the basis of spectral IP measurements. However, we believe that the sandstones featuring 'slow' diffusion can be discriminated based on the integral polarization parameters, and that the relaxation time remains a valuable parameter for assessing hydraulic properties of clean sandstones.

Key words: Electrical properties; Hydrogeophysics; Permeability and porosity.

1 INTRODUCTION

Information regarding permeability of rocks is essential in understanding and modelling flow of liquids in reservoirs, including oil exploration and groundwater investigation. In the last decade, attempts have been made to assess hydraulic properties of soils and sediments on the basis of measurements of the complex electrical conductivity (resistivity) or complex dielectric constant (e.g. Börner *et al.* 1996; Lesmes & Morgan 2001; Scott & Barker 2003; Scott 2004; Binley *et al.* 2005). This approach is called electrical spectroscopy or spectral induced polarization (IP).

In ion-conductive sandstones, the imaginary component of the complex electrical conductivity is related to an electrical double layer (EDL) surrounding mineral grains. Because of excess of cations and deficiency of anions typical of the EDL, the passage of an electrical current produces local ion concentration gradients, which result in the membrane (diffusion) potential (e.g. Marshall & Madden 1959; Dukhin & Shilov 1974). The membrane potential is out of phase with respect to the polarizing electrical current. The time it takes ions in the EDL to return to the equilibrium after the polarizing current is cut off is the relaxation time. Because of the diffusive origin of this phenomenon, the relaxation time is

proportional to the square of the average ion displacement length (e.g. Schwarz 1962; Kormiltsev 1963; Lesmes & Morgan 2001; Titov *et al.* 2002). The distribution of the ion displacement lengths, related to distributions of grain sizes or pore throat lengths, defines the relaxation time distribution (RTD).

In previous works, IP-derived data (e.g. RTD or the parameters of the electrical conductivity spectra) were compared with non-electrical data [e.g. volumetric grain size distribution, Mercury Injection Capillary Pressure (MICP) data, and permeability].

In the study of Berea sandstone samples, Lesmes & Morgan (2001) obtained RTD by inverting the real part of the dielectric constant. For this inversion, they used the generalized Debye polarization model. They based the inversion on the regularized solution of the Fredholm integral equation of the first kind, which relates the complex dielectric constant spectrum, $\varepsilon^*(\omega)$, to the relaxation time distribution, $g(\tau)$ (Morgan & Lesmes 1994)

$$\varepsilon^*(\omega) = \varepsilon'_\infty + (\varepsilon'_0 - \varepsilon'_\infty)\int_0^\infty \frac{g(\tau)}{1 + \mathrm{i}\omega\tau}\mathrm{d}\tau, \quad (1)$$

where ε'_∞, ε'_0 are the high frequency and low frequency limits of the dielectric constant, respectively; ω is the angular frequency; τ is the relaxation time.

Lesmes & Morgan (2001) related RTD to the volumetric grain size distribution. As far as we know, they were the first to propose an assessment of the grain size distribution based on the RTD.

Scott & Barker (2003) studied samples of Permo-Triassic sandstone from the UK. Applying the MICP method, they found that the distributions of pore throat diameters for their samples were unimodal, that is, for each sample there was a most probable value of the diameter. We call this value, d_0, 'the modal pore-throat diameter'. In contrast to Lesmes & Morgan (2001), Scott & Barker (2003) simply correlated positions of peaks in the electrical conductivity phase spectra, f_{peak}, with the pore throat diameter, d_0. They found an inverse correlation between f_{peak} and d_0.

Later, Scott & Barker (2005) obtained the relaxation time, τ, by fitting their experimental data with the generalized Cole–Cole model (Dias 2000). With this improved procedure, they obtained a positive correlation between τ and d_0.

Binley *et al.* (2005) studied electrical–hydraulic relationship in Sherwood Sandstone samples. They fitted the experimental complex electrical conductivity spectra with the Cole–Cole resistivity model (Pelton *et al.* 1978). For water-saturated sandstones, they showed a positive correlation between the model relaxation time and the hydraulic conductivity. They also found a positive correlation between the relaxation time and the pore throat diameter.

Tong *et al.* (2006) conducted time domain (TD) measurements on shaley sands. Unlike in the conventional frequency domain (FD) measurements, which use the harmonic current wavelength form, in TD, the current wavelength form is typically a series of pulses of the various durations and opposite polarities. Tong *et al.* (2006) inverted IP decays to RTD on the basis of a singular-value decomposition. Then they assessed MICP distributions from RTD by (1) calculating cumulative RTD curves, and (2) rescaling the cumulative RTD curves using empirical coefficients. They showed a good fit between the true and IP-derived MICP curves.

Tarasov & Titov (2007) extended the inversion algorithm of Morgan & Lesmes (1994) for TD data. They tested the algorithm on synthetic data and obtained experimental RTDs for sieved sands and sand mixtures. For sieved sands, they found unimodal RTDs. For sand mixtures containing two grain sizes, they found both unimodal and bimodal RTDs depending on the grain size distributions. Comparing the sand granulometric compositions with the RTDs, they related RTD peak positions to grain size distributions. Henceforth, we call the RTD peak position 'the modal relaxation time', τ_0.

Kruschwitz *et al.* (2009) analysed a number of previously obtained and new spectral IP data sets on the basis of the generalized Cole–Cole resistivity model (Pelton *et al.* 1983). For samples containing mostly large pore throats, they found that the relaxation time increased with the increase of the modal pore throat size. For samples mostly containing small pore throats, they found no relationships between the relaxation time and the modal pore throat diameter. Kruschwitz *et al.* (2009) concluded that 'for such media the microstructure of the network of small pores leads to some connectivity of diffusion path and thus this samples exhibit relatively long relaxation times'.

Summarizing state-of-the-art of the spectral IP method, we would like to emphasize an increasing interest to using the method as a tool for assessing hydraulic and physical–chemical properties of sediments and soils. However, the value of the method is limited by insufficient experimental database, which leads to incomplete understanding of the IP mechanism. Therefore, the main goal of this paper is to extend the factual database. Also, most of the experimental data to date were obtained using FD measurements, while in the field the TD technique is used much more often. There are few petrophysical data obtained in the TD mode to date. These data describe unconsolidated soils (Titov *et al.* 2002; 2004; Tarasov & Titov 2007), and only one data set involves rocks (Tong *et al.* 2006). Therefore, another goal of this paper is to demonstrate the feasibility of spectral IP approach on the basis of the TD technique.

2 METHODOLOGY

This paper describes electrical data obtained from TD IP measurements on six sandstone samples. To compare electrical properties of sandstones with physical–chemical properties commonly used in hydrogeology and in the oil industry, we also measured the sample porosity, permeability, specific surface area (SSA) and MICP distributions. The samples have contrasting mineralogical characteristics (Table 1). The two central parameters for transport properties, porosity and clay content, vary from 19 to 26 per cent (Table 2) and from 4 to 31 per cent (Table 1), respectively. This leads to a wide range of hydraulic conductivity (from 0.42 to 1091 mD).

Table 1. Mineralogical composition of the studied samples (in weight per cent).

Sample	Quartz + Chert	Feldspar	Carbonate	Clay	Evaporite
Berea 100	85.0	4.4	3.9	6.1	0.4
Berea 400	89.2	3.9	1.1	5.2	0.4
Boise 264	46.8	45.2	0.8	6.4	0.5
Massilon 1065	90.5	0.0	3.9	3.7	0.4
Portland	36.6	9.1	22.6	31.2	0.1
Bandera 274	58.6	13.7	1.1	20.2	1.5

Table 2. Physical–chemical properties of the studied samples SSA is the specific surface area; F is the formation factor; d_0 is the modal pore throat diameter.

Sample ID	Porosity (per cent)	Permeability (mD)	SSA ($m^2\ g^{-1}$)	F	d_0 (μm)
Berea 100	20.2	258	1.01	18.8	12.0
Berea 400	23.6	843	0.81	14.0	23.6
Boise 264	25.6	604	0.77	13.7	15.6
Massilon 1065	22.0	1091	1.52	12.9	33.0
Portland	18.9	0.42	3.29	19.7	0.42
Bandera 274	20.8	19.4	2.64	11.9	6.22

We inverted the TD IP data to RTD using an algorithm proposed by Tarasov & Titov (2007), and we analysed relationships between the aforementioned physical–chemical properties and the electrical properties.

2.1 Sample preparation and succession of measurements

First, an optimal experiment protocol was established using two Berea sandstone samples (Amherst, Ohio, Cleveland quarries). These samples (and subsequently all other samples) were cleaned using the Soxhlet method (Soxhlet 1879) with successive extraction in toluene, acetone and chloroform. After drying for 24 hr at 60 °C, two Berea sandstone samples were saturated with 5 Sm^{-1} NaCl (at 25 °C) solution using the vacuum/pressure saturation method, and the first series of IP measurements were carried out. The salinity for the first saturation was chosen to resemble the values characteristic of some brines found in oil-bearing formations. After the first series of measurements, two Berea sandstone samples were placed in individual 200 ml containers filled with distilled water and left to equilibrate to a new salinity state. The electrical conductivity of water was monitored against time in order to control diffusion of the salt from samples to the surrounding solutions. The conductivity of water gradually increased, indicating salt movement from the samples to the equilibration container. After a certain time, water conductivities reached constant values characteristic of the new equilibrium state. This procedure is further referred to as the 'desalinization' because it results in decrease of the salt concentration in the samples. The desalinization procedure took four months until the new equilibrium brine electrical conductivity of 0.2 Sm^{-1} for both samples was reached. After that, the second set of IP measurements was carried out.

Because the desalinization procedure took a long time, four other samples (Boise sandstone, Massilon sandstone, Portland sandstone and Bandera sandstone), were saturated directly with 0.2 Sm^{-1} NaCl solution. After that the IP measurements were carried out on these four samples. Then, they were desalinized using the described procedure. The new equilibrium water conductivity for these samples was approximately 5.9×10^{-2} Sm^{-1}. After measuring the IP response of the desalinized samples, the samples were vacuum-saturated with NaCl brine of 4.31 Sm^{-1}, and the IP measurements were carried out again.

2.2 Non-electrical measurements

The non-electrical sample characterization included measurements of the core porosity, gas permeability, specific surface area and MICP. The details of the characterization methods are given below.

(1) Gas permeability measurements were carried out on cylindrical plugs 3.81 cm long and 3.81 cm in diameter, using an automated gas permeameter developed at Schlumberger-Doll Research (US Patent #5832409).

(2) Specific surface area measurements were made on plugs using the BET method (Brunauer *et al.* 1938) with the Micromeritics Gemini 2360 analyser. This instrument uses a flowing-gas technique, in which the adsorptive nitrogen gas flows into the sample and the balance tubes at the same time. A pressure transducer monitors the pressure between the two reservoirs to determine the amount of gas that is adsorbed on the sample. Due to the limited tube size, only the plugs 0.75 cm in diameter were measured.

(3) The pore throat size distributions were obtained using the MICP method. The method allows evaluation of the pore throat size distribution by measuring mercury intrusion into the sample at a variable pressure. As the pressure increases, mercury enters the pores beginning with those of the largest diameter. Pore throat size is calculated for each pressure value, and the corresponding volume of mercury required to fill these pores is measured. These measurements, taken over a range of pressures, result in the 'pore volume versus pore size' distribution for the sample material (Purcell 1949).

2.3 Electrical measurements

Electrical measurements were carried out on plugs 3.81 cm long and 3.81 cm in diameter. We used a measuring cell similar to that described in Binley *et al.* (2005).

2.3.1 Apparatus and procedure

For the TD IP measurements, we used the AIE-2 instrument (www.elgeo.ru), and a laboratory transmitter that allowed injection of stabilized current into the sample The most important feature of the approach is the dense decay sampling (tens to hundreds points per decay). For more details concerning the measurement setup and instrument, see Titov *et al.* (2002, 2004) and Tarasov *et al.* (2003).

For the TD IP measurements, we used the following protocol. Three current wavelengths were used: 2, 10 and 99 s, with the equal durations of pulses and pauses. Use of the various current wavelengths for improving the quality of the TD IP data was described in previous papers (Soininen 1984; Johnson 1984; Lewis 1985). Moreover, it was shown that the use of three current wavelengths enables strong improvement of RTD assessments (Tarasov & Titov 2007). The IP voltage was sampled in time windows, and the voltages per window were averaged. With this approach, the wider the window, the greater the signal-to-noise ratio. Short pulses ($T = 2$ s) were used for studying early parts of the IP decays. For short pulses, narrow time windows were used. The signal-to-noise ratio was improved by stacking the responses over 10 pulses. Increase of the pulse duration ($T = 10$ and 99 s) resulted in wider time windows,

which allowed keeping a reasonable signal-to-noise ratio with reduced number of stacked responses.

2.3.2 Inversion of recorded decay curves to relaxation time distribution

Inversion of the decays to RTD is based on the equation relating the dimensionless polarizability, $\eta(t)$, with the density of RTD, $g(\tau)$ (in s^{-1})

$$\eta(t) = \int_0^\infty g(\tau)F(t/\tau, T, NI)\mathrm{d}\tau. \quad (2)$$

Here $F(t/\tau, T, NI)$ is the dimensionless theoretical IP decay, which is the convolution of the presumed IP decay characteristic of a polarizing element of the rock texture, $F(t/\tau)$, with the current waveform, $I(t_0)$,

$$F(t/\tau, T, NI) = \int_0^t I(t_0, T, NI) \cdot F\left(\frac{t - t_0}{\tau}\right)\mathrm{d}t_0, \quad (3)$$

where t_0 is the integration variable, and NI is the number of the stacked pulses.

Eq. (2) is based on superposition of the responses of polarizing elements distributed with the probability density, $g(\tau)$. The elements have a relaxation described by the $F(t/\tau)$ rule, and they are polarized by the current with the wavelength form $I(t_0, T, NI)$.

For the Debye relaxation model $F(t/\tau)$ is the damped exponential,

$$F(t/\tau) = \exp\left(-\frac{t}{\tau}\right). \quad (4)$$

By introducing a new variable, $Z(s)$, instead of $g(\tau)$ on the basis of normalization (5), and the transformation of variables (6) and (7)

$$\int_0^\infty g(\tau)\mathrm{d}\tau = \int_{-\infty}^\infty Z(s)\mathrm{d}s = \eta_0, \quad (5)$$

$$s = \ln(\tau), \quad (6)$$

$$p = \ln(t), \quad (7)$$

the new model function is defined

$$\Phi(p - s, T, NI) = F(t/\tau, T, NI). \quad (8)$$

Using these new variables, Tarasov & Titov (2007) presented eq. (2) in the form

$$\eta(p) = \int_{-\infty}^\infty Z(s)\Phi(p - s, T, NI)\mathrm{d}s. \quad (9)$$

Note that the density, $g(\tau)$, is expressed in s^{-1} (eq. 2), while $Z(s)$ is a dimensionless parameter (eq. 9). This parameter, characterizing RTD, will be interpreted thereafter. Eq. (9) is the Fredholm equation of the first kind, which is an ill-posed problem. The Tikhonov regularization approach (Tikhonov & Arsenin 1986) was applied to solve it. For more details about the inversion procedure, see Tarasov & Titov (2007).

In this study, we used two model functions $F(t/\tau)$. First, we obtained RTD on the electrical circuit measurements applying the Debye relaxation model (eq. 4). Then, for the data obtained on the samples, we applied a so-called 'short narrow pore' (SNP) model of polarization, describing the electrical relaxation of a pore throat (Titov *et al.* 2002). It is presented in TD by the following equation:

$$F\left(\frac{t}{\tau}\right) = \frac{1}{\sqrt{\pi}}\sqrt{\frac{t}{\tau}}\left[1 - \exp\left(-\frac{\tau}{t}\right)\right] + \mathrm{erfc}\left(\sqrt{\frac{\tau}{t}}\right). \quad (10)$$

2.3.3 Calibration experiments

Two calibration tests of the experimental setup were performed. First, a 'blank' water test was carried out using water with three different electrical conductivity values (0.29, 0.050 and 0.014 Sm^{-1}). These values roughly correspond to the conductivity of the samples saturated with water of different salinities. This test was performed in order to check the capacitive coupling, which is a characteristic of four-electrode arrays (e.g. Lesmes & Frye 2001), and the stability of the non-polarizing potential electrodes. Second, a test on electrical circuits was carried out. Circuits contained a serial connection of a resistance R_0, and an RC-contour (which is a parallel connection of a resistance, R, and a capacitance, C). These circuits provide relaxations with *a priori* known values of the time constant, $\tau = RC$. This test was done in order to verify the accuracy of the relaxation time obtained with our approach. Thereafter, we call this test 'RC-test'.

Fig. 1 shows the results of the 'blank' water test. The observed decays represent the assembly noise, which must be significantly lower than the sample responses. The IP decay obtained on the Bandera 274 sample, saturated with saline water (when the lowest IP response) is also shown for comparison. For the 'blank' test with fresh water (0.014 Sm^{-1}), with the highest (in our series of tests) capacitive coupling, starting from 0.01 s, the decay values are less than 5 per cent of the values obtained on the sample. Therefore, at least in the time range over 0.01 s, we can disregard the noise produced by the capacitive coupling.

The largest resistance of the samples was about 15 kOhm. In the RC-test, we modelled the Ohmic resistivity of the samples using a circuit with the resistance of 20 kOhm. We used the different capacitances to obtain the various relaxation time values. The circuits provided three values of the relaxation time: 2×10^{-1}, 2×10^{-2} and 2×10^{-3} s. Fig. 2 shows the measured decays obtained with the protocol described above. The decays corresponding to three values of the relaxation time are similar in shape, but are mutually shifted. The longer the calculated relaxation time, the more the decay is shifted to the right along the time axis. Performing inversion of the RC test data according to the Debye relaxation model, we obtained a good correspondence between the observed peaks in the RTD and the theoretical relaxation values (Fig. 3).

3 RESULTS

3.1 Non-electrical measurements

Characterization of the six sandstone samples by non-electrical measurements revealed that the collection represented samples of different mineralogical composition and physical properties. The mineralogical characteristics of the samples are summarized in Table 1.

Examples of MICP curves are shown in Fig. 4. The modal pore throat diameter for the studied samples varies between 0.4 and 40 μm. For five samples, unimodal distributions were found, and

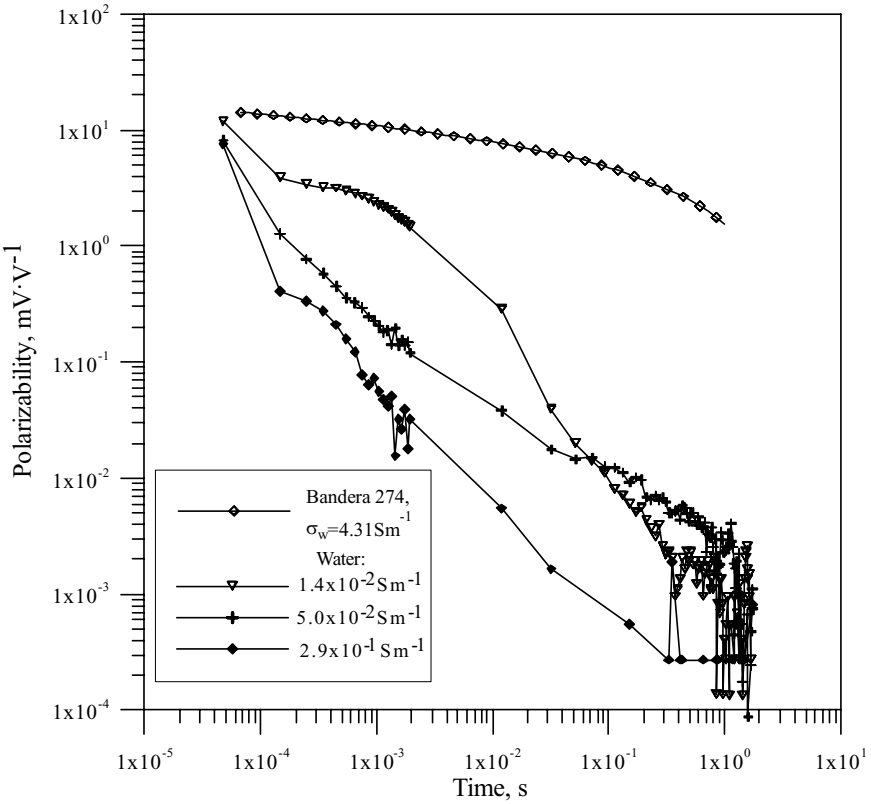

Figure 1. IP decays obtained in the 'blank' water test. Numbers show the values of the water electrical conductivity. Data obtained on the Bandera 274 sample, saturated with saline water ($\sigma_w = 4.31\ Sm^{-1}$), are shown for comparison.

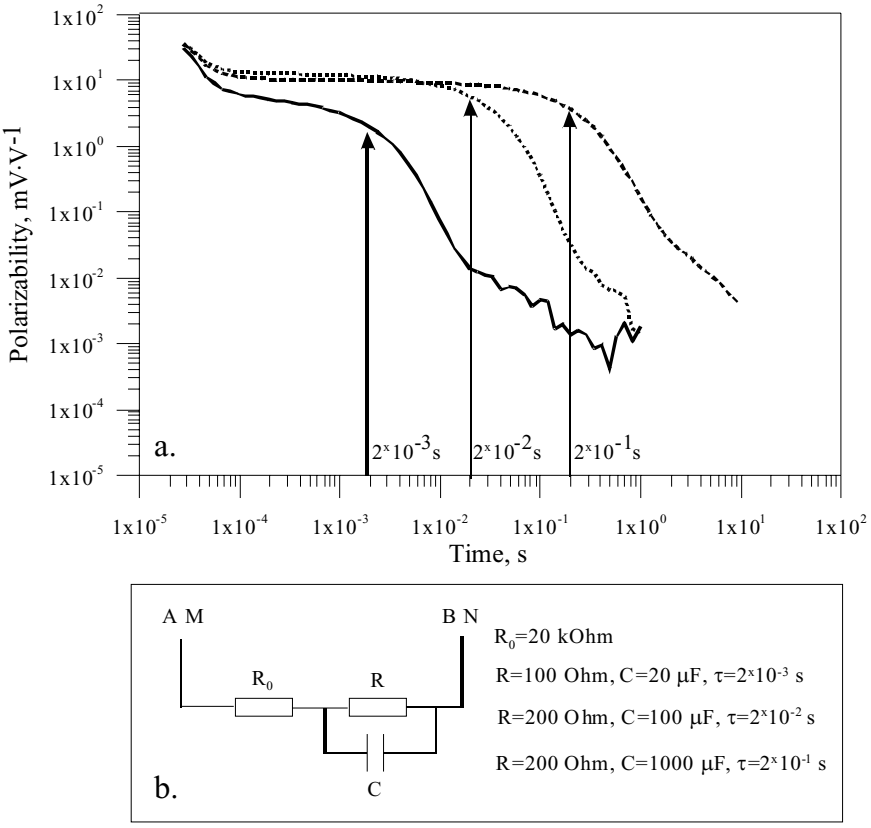

Figure 2. IP decays (a) obtained on electrical circuits (b) containing resistances and capacitances providing relaxations with *a priori* known values of the time constant (RC-test).

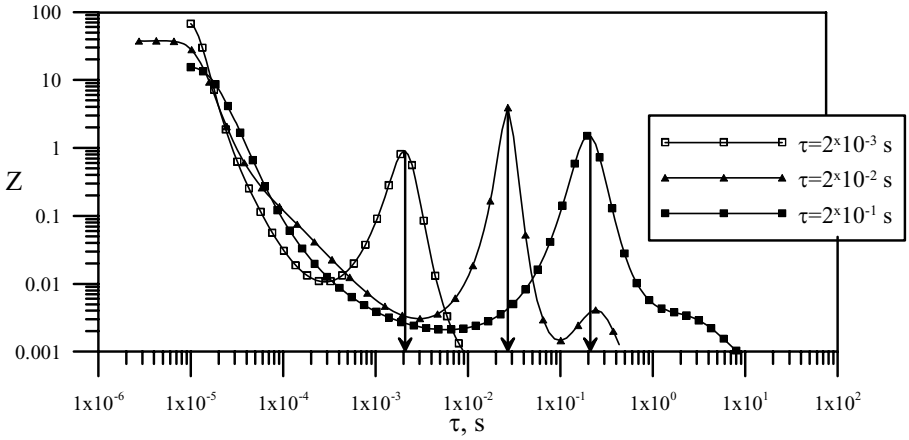

Figure 3. Relaxation time distributions obtained from RC-test.

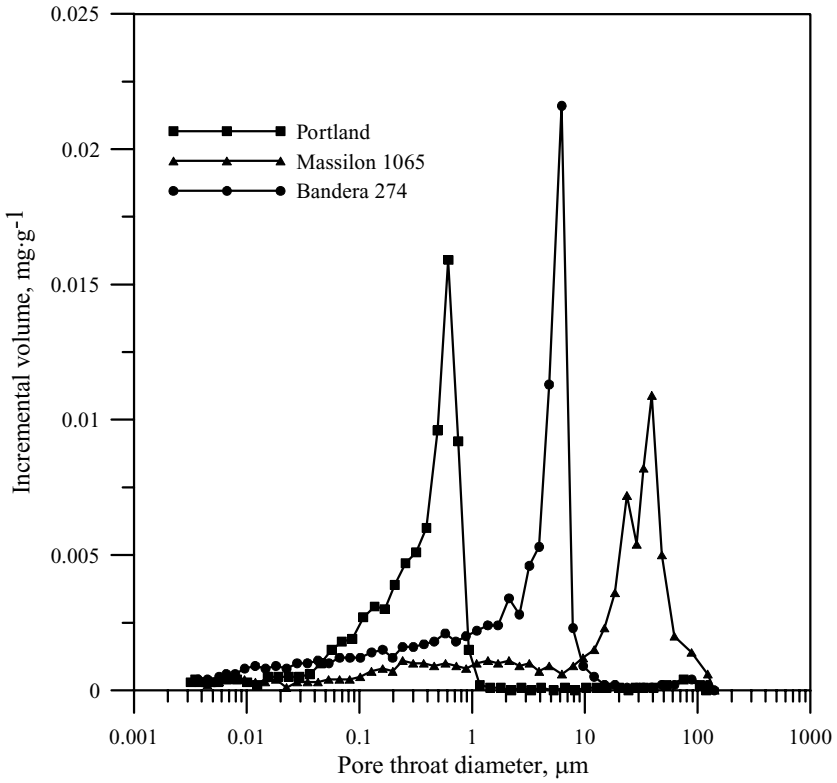

Figure 4. Examples of the mercury injection capillary pressure data.

for one sample (Masillon 1065), the distribution was found to be bimodal, with two peaks located at 18 and 33 μm.

Physical–chemical properties of the studied samples are summarized in Table 2.

Fig. 5 shows relationships between the physical–chemical characteristics of the samples. Permeability and the modal pore throat diameter are in strong positive power relationship (Fig. 5a). The permeability is inversely correlated with SSA (Fig. 5b), and SSA is positively correlated with the clay content (Fig. 5c). Also the modal pore throat diameter is inversely correlated with the clay content, which suggests that small pore throats are formed by clay particles or filled with clay (Fig. 5d). Therefore, for our collection, the permeability is controlled by both the pore throat diameter and the clay content.

3.2 Electrical measurements

Fig. 6 shows an example of IP decays obtained on the Bandera 274 sample saturated with water of three electrical conductivity values. It is seen that the magnitude of the polarization decreases with the water conductivity increase. However, even at the highest

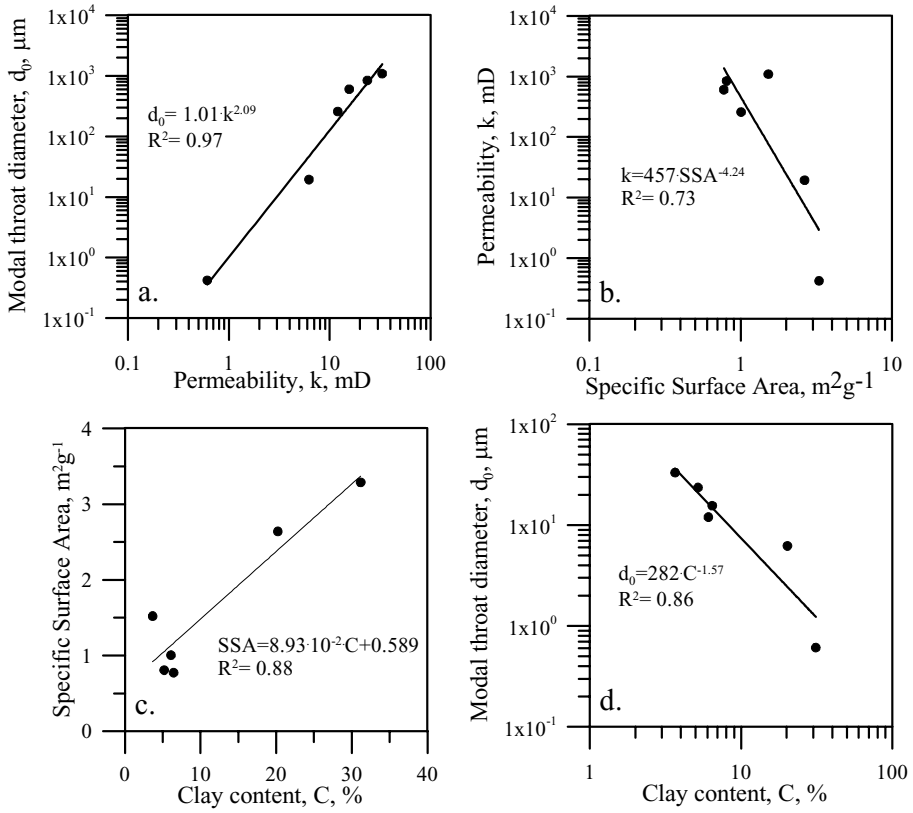

Figure 5. Relationships between physical–chemical properties of the samples: (a) the modal pore throat diameter versus permeability; (b) permeability versus the specific surface area; (c) the specific surface area versus the clay content; (d) the modal pore throat diameter versus the clay content.

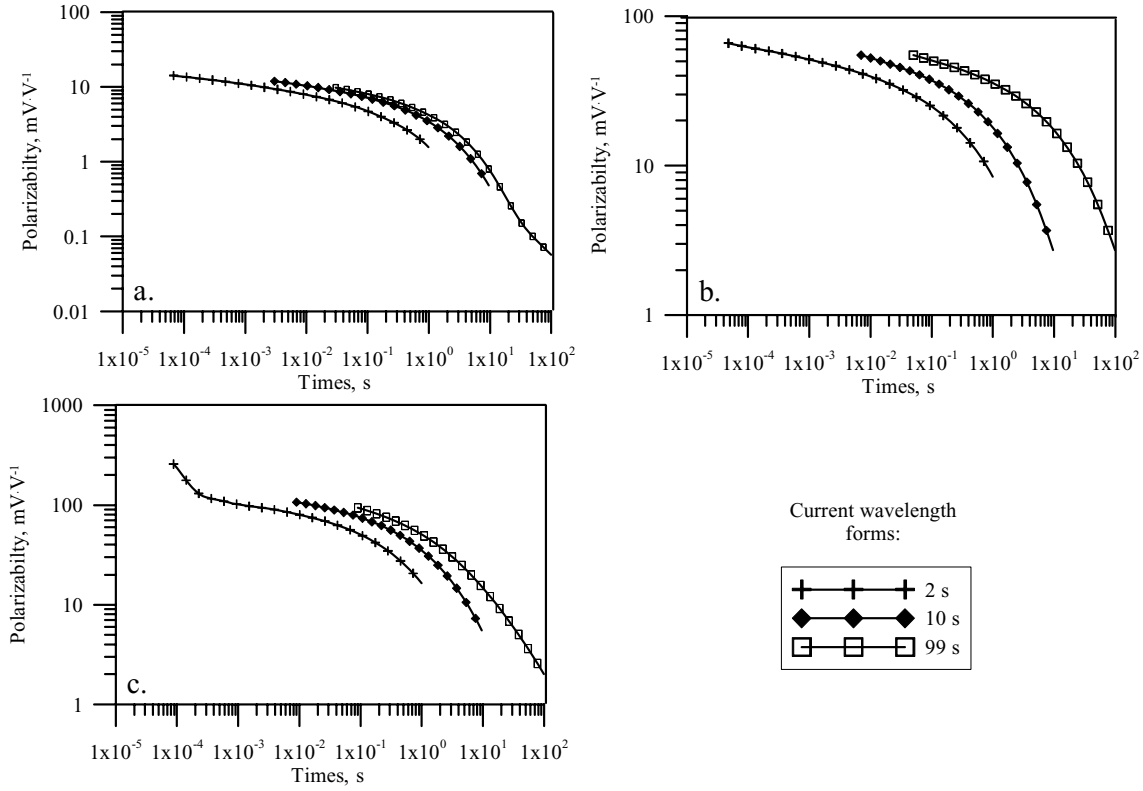

Figure 6. Examples of IP decays obtained on the Bandera 274 sample saturated with water of the various electrical conductivity: (a) 4.31 Sm^{-1}, (b) 0.20 Sm^{-1} and (c) 3.94×10^{-2} Sm^{-1}.

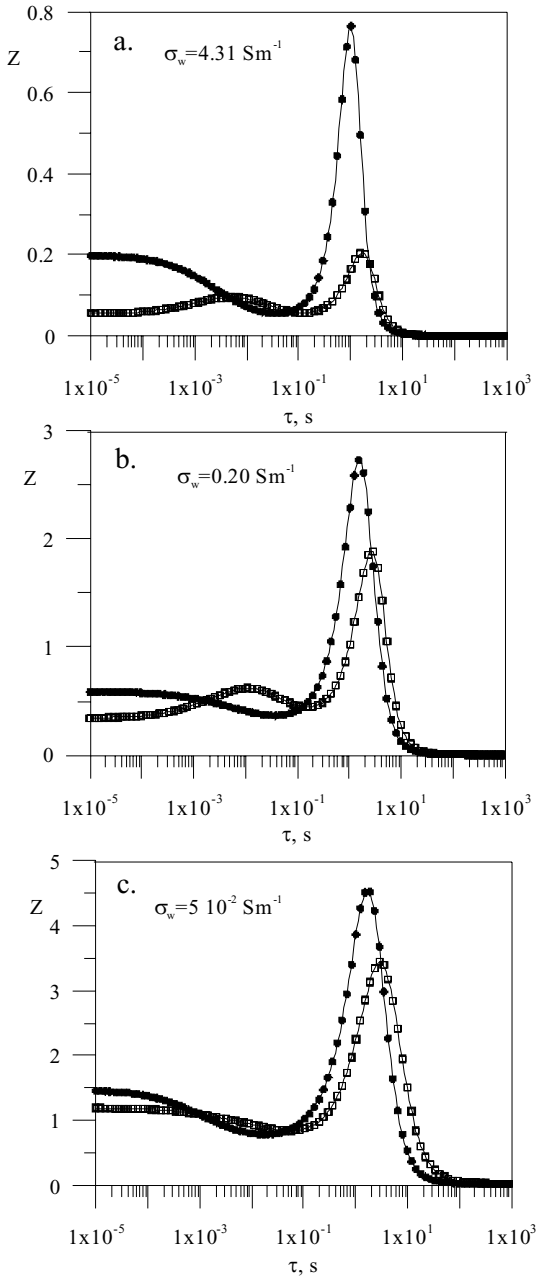

Figure 7. Relaxation time distributions obtained on samples Bandera 274 (filled circles) and Boise 264 (open squares) saturated with water of the various electrical conductivity [(a) 4.31 Sm^{-1}, (b) 0.20 Sm^{-1}, (c) about 0.05 Sm^{-1}]. The inversion was based on the SNP model.

conductivity value, and for a late time range (about 99 s), the polarizability is an order of magnitude greater than the level of noise (Fig. 1).

Fig. 7 shows examples of RTD inversion obtained on samples Bandera 274 and Boise 264 saturated with water of different electrical conductivities. We used the model function describing the SNP model (eq. (10)). All distributions contain peaks in the time range from 1 to 25 s.

Integral parameters of the electrical data are summarized in Fig. 8. We calculated chargeability corresponding to the pulse of the longest duration (99 s). The chargeability was found to be a decreasing function of the water electrical conductivity (Fig. 8a). Normalized chargeability, which is a measure of the net polarization effect, was calculated from the chargeability, η, and the water electrical conductivity, σ_w (e.g. Lesmes & Frye 2001)

$$MN = \eta\sigma_w. \tag{11}$$

The normalized chargeability was found to be a slightly increasing function of the water electrical conductivity (Fig. 8b).

The relationships between the modal relaxation time, τ_0, and the water electrical conductivity (Fig. 8c) are different for the different samples. For three samples (Portland, Boise 264 and Bandera 274) τ_0 shows a weak dependence on the water conductivity. For two samples (Berea 100 and Berea 400) τ_0 slightly increases with the water conductivity increase. In all these cases, the ratio of τ_0 at high electrical conductivity to τ_0 at medium conductivity is within the range from 0.57 to 3.3. Conversely, for the Massilon sample, τ_0 is almost constant at low and medium conductivity values, and then decreases by an order of magnitude at the highest conductivity value.

Fig. 9 shows relationships between the normalized chargeability and the volumetric clay content for high and medium water conductivities. For these relationships, we found positive correlations, which confirm that for our samples the polarization is at least partially controlled by the clay content.

Taking in consideration the aforementioned behaviour of the relationship $\tau_0(\sigma_w)$, we tend to view the relationship between the modal pore throat diameter and the relaxation time in the following way. First, we tried obtaining a regression for the entire data set. However, this proved unsuccessful. Then, we based our analysis on the geometrical mean value of the modal relaxation times obtained by measuring a sample saturated with water of different electrical conductivities, $\bar{\tau}$, which is called thereafter 'the characteristic relaxation time'. Fig. 10(a) shows the relationships between the modal pore throat diameter, obtained from the MICP data, and the characteristic relaxation time, $\bar{\tau}$. A positive logarithmic dependence,

$$d_0 = 16.8 \ln \bar{\tau} - 2.15, \tag{12}$$

fits the data well (in eq. (12) d_0 is expressed in μm, and $\bar{\tau}$ – in s). The logarithmic relationship is in agreement with the results obtained by Scott & Barker (2003), however the coefficients are different. If the characteristic diffusion length is considered proportional to the pore throat diameter or, alternatively, to the grain diameter, the logarithmic relationship is in disagreement with the existing theories (e.g. Schwarz 1962; Kormiltsev 1963; Titov *et al.* 2002), which predict a power-law relationship between the characteristic diffusion length, l, and the relaxation time

$$l \sim \sqrt{D\tau}, \tag{13}$$

where D is the ion diffusivity. The relationship between the permeability, k, and $\bar{\tau}$ (Fig. 10b) also fits the logarithmic law well with the coefficient of determination value slightly lower than that for the previous case. This is directly explained by the correlation between d_0 and k shown in Fig. 5(a).

4 DISCUSSION

The chargeability was found to be a decreased function of the water electrical conductivity (Fig. 8a), which is in agreement with previous works (e.g. Lesmes & Frye 2001).

The normalized chargeability, MN, was found to be a slightly increased function of the water electrical conductivity (Fig. 8b),

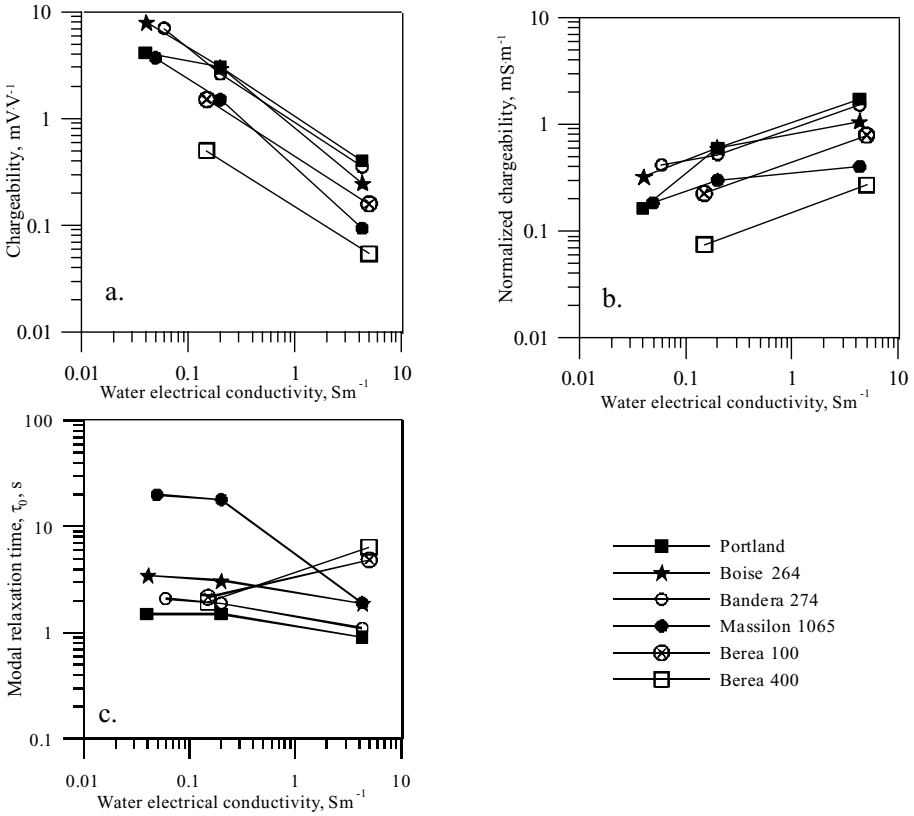

Figure 8. Electrical parameters versus brine electrical conductivity: (a) chargeability, (b) normalized chargeability and (c) the modal relaxation time.

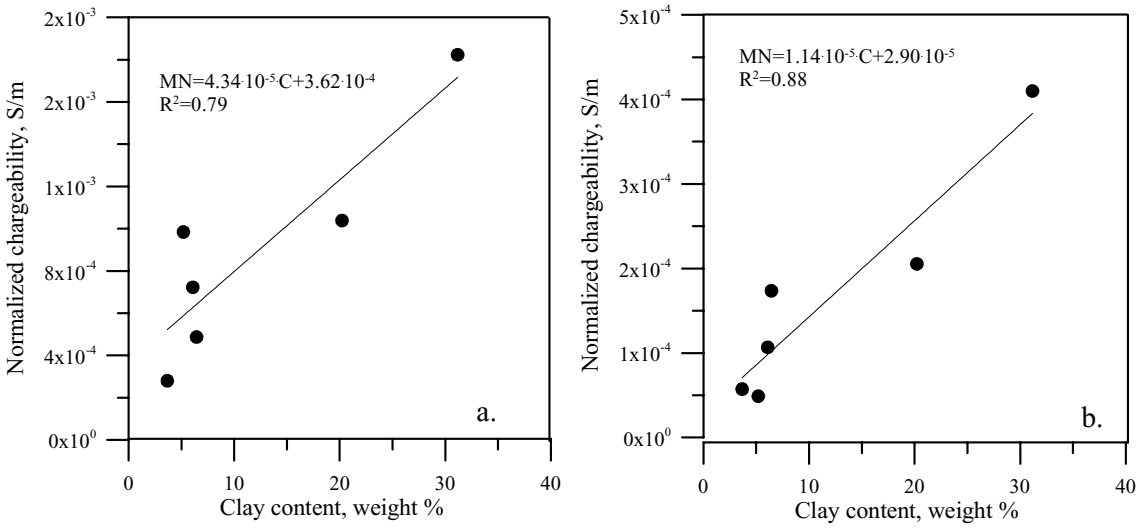

Figure 9. Normalized chargeability versus volumetric clay content for the samples saturated with water of high (a) and medium (b) salinity.

which agrees with the data presented by Scott (2004), and disagrees with the data by Lesmes & Frye (2001). Lesmes & Frye (2001) found that the dependence of MN on σ_w contains a maximum. They proposed that the increase of MN in the low conductivity range is related to the increase of the surface charge density with increase of the solution concentration. They related the decrease of MN in the high conductivity range to the ion-ion interactions, which cause the effective surface ionic mobility to decrease at high salinity values. The concurrency between these two mechanisms produces a relationship containing a maximum. Lesmes & Frye (2001) found the maximum of the $MN(\sigma_w)$ relationship at about 1 Sm^{-1}. However, the position of the maximum can also depend on properties of the solid-liquid interface, and on the chemical composition of the pore water. We believe that for the data of Scott (2004), as well as for our data in the studied electrical conductivity range, the increase of the surface charge density is the dominant mechanism, which controls the integral polarization effect. The maximum for our collection, therefore, may be shifted right, to higher values of the water electrical conductivity. This hypothesis is in agreement with results of Flath (cited by Scott 2004), where

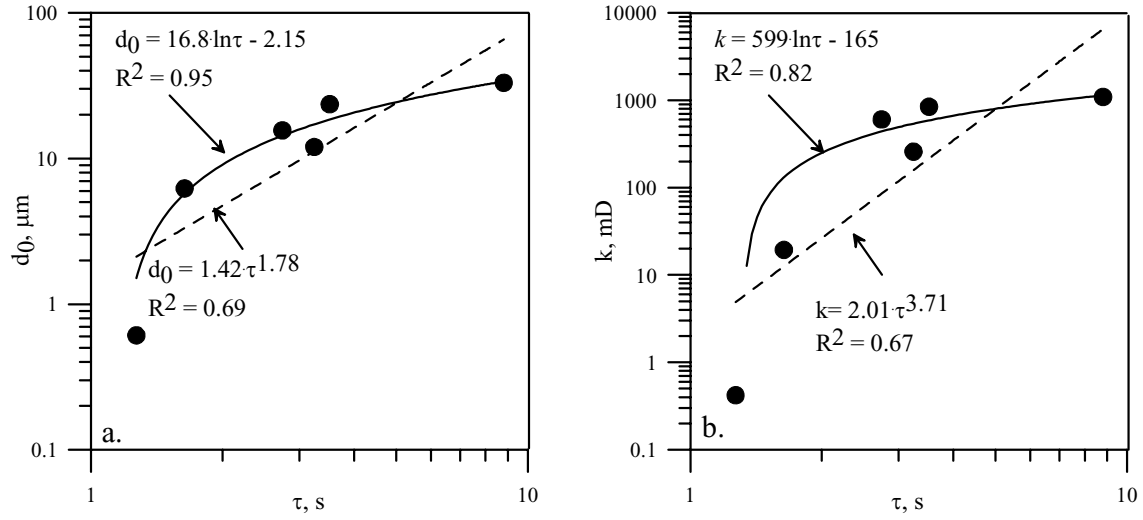

Figure 10. Relationships between: (a) the modal pore throat diameter, d_0, and the characteristic relaxation time, $\bar{\tau}$; (b) between permeability, k, and the characteristic relaxation time. Solid lines and dashed lines show logarithmic and power best fits, respectively.

the maximum was found at the water conductivity value of about 5 Sm^{-1}.

The normalized chargeability shows a positive linear correlation with the clay content (Fig. 9). The clay content also negatively correlates with the pore throat diameter (Fig. 5d). We consider, therefore, the clay particles as the polarizing elements in the sandstones, and suggest that at least part of the pore throats is filled with clay.

The relationship between the modal relaxation time and the water electrical conductivity (Fig. 8c) is contradictory. In three samples τ_0 was found to be almost independent of the water conductivity. Two samples show slightly increased values of τ_0 at higher conductivities. This increase of τ_0 may be related to the decrease of the ion mobility with the increase of the water electrical conductivity [and, consequently, the decrease of the diffusivity, see eq. (13)].

One sample (Massilon 1065) shows a tenfold decrease of $\tau_0$when the water conductivity decreases from 0.2 to 4.31 Sm^{-1} (Fig. 8c). We propose two hypotheses to explain this behaviour. On the one hand the MICP distribution for this sample is bimodal: the peaks were found at 33 and 18 μm (Fig. 4). Tarasov (2008) showed theoretically that the magnitude of polarization of a pore throat is an extremal function of the water salinity and the pore throat size. Therefore, in principle, depending on the water salinity, less frequent pore throats may produce larger polarization effect than the dominant pore throats. The shift of the polarization effect to smaller pore throats explains the shift of τ_0 to lower values. However, taking in consideration the modal pore throat diameters characteristic of the Massilon 1065 sample and eq. (13), we can predict the shift of τ_0 by a factor of 3.4, but not by a factor of 10. Therefore, this 'shift' effect cannot completely explain the relationship between τ_0 and σ_w.

On the other hand, the Massilon 1065 sample has the highest value of d_0 and the lowest clay content in our collection. Therefore, the polarizing elements for the sample are the pore throats filled with water. Because of this, the chargeability in this sample at high water conductivity value is the lowest in the collection, and the error of determination of the relaxation time distribution is the highest. It is possible that both discussed factors (the 'shift' effect as well as a relatively large error in determination of τ_0) contribute to the unusual observed behaviour of $\tau_0(\sigma_w)$.

Now we discuss the relationship between the characteristic relaxation time and the pore throat diameter. Eq. (12) is of limited value

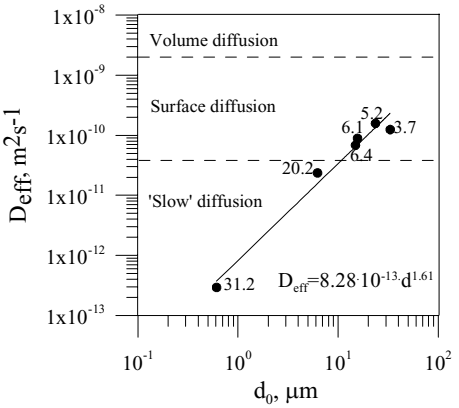

Figure 11. Effective diffusivity versus modal pore throat diameter. The filled circles show the IP and MICP derived data, and the solid line shows the best power-law fit. The numbers indicate the clay content.

for the estimation of d_0 because it may produce negative values of the modal pore throat diameter and, therefore, it is only valid for a limited range of the characteristic relaxation time ($\bar{\tau} > 1.13$ s for our collection). Therefore, eq. (12) is not universal. Also, the logarithmic dependence is in disagreement with the theoretical prediction, eq. (13).

To interpret our data, we adopted approach of Kruschwitz *et al.* (2009). Accordingly, we considered the diffusivity in eq. (13) as a variable, which is calculated from the modal pore throat diameter and the characteristic relaxation time,

$$D_{\text{eff}} = \frac{d^2}{\bar{\tau}}, \tag{14}$$

so that the large relaxation time is related to the 'slow' diffusion. We fit our data assuming a power-law relationship $D_{\text{eff}} \propto d_o^n$ (Fig. 11). For our collection, we obtain three orders of magnitude variation in effective diffusivity. The value of power that we found is in a remarkable agreement with the results obtained by Kruschwitz *et al.* (2009): 1.61 for our collection and 1.68 for their collection. Kruschwitz *et al.* (2009) related the variation of the effective diffusivity to the variation of the specific surface area and the

formation factor: low values of the effective diffusivity correspond to high values of the formation factor and specific surface area. For our collection, we found an inverse correlation of the effective diffusivity with the specific surface area ($R^2 = 0.76$) and with the clay content ($R^2 = 0.90$).

Revil (1999) calculated values of the surface diffusivity on the basis of the electrical conductivity measurements. He found the following values: from 3.9×10^{-11} m^2 s^{-1} (for Cs^+) to 4.1×10^{-10} m^{2}s^{-1} (for H^+). For our collection, in the clay content range from 3.2 to 6.4 per cent, the effective diffusivity values (from 6.8×10^{-11} to 1.6×10^{-10} m^2 s^{-1}) are characteristic of the surface diffusion. For this case, we consider the surface diffusion along the boundaries of the pore throats not filled with clay. For higher clay content, the effective diffusivity values decrease up to 2.9×10^{-13} m^2 s^{-1}, which is two orders of magnitude lower than that for the surface diffusivity.

We propose two mechanisms that may explain this 'slow' diffusion.

(1) *Surface tortuosity effect:* In the pores filled with clay, the effective surface diffusivity is reduced because the clay mineral surface is rough (see micrographs, e.g. in Martil *et al.* 2003). The reduction of the surface diffusivity may be described in terms of surface tortuosity of clay, in a similar manner as the reduction of the bulk electrical conductivity in porous media is described in terms of volume tortuosity,

$$D_{\text{eff}} = D_s/\vartheta_s^2, \tag{15}$$

where ϑ_s is the surface tortuosity of clay, and D_s is the surface diffusivity.

(2) *Pore geometry effect:* In this paper, we calculated the effective diffusivity based on the characteristic relaxation time and modal pore throat diameter. However, the diffusivity must be calculated from the characteristic diffusion length (that is, from the length of a pore throat). In the other words, using eq. (14), we considered that the pore throat length is equal to the pore throat diameter. Assuming, in contrast, a 'long' pore with a length

$$l = ad_0, \tag{16}$$

where a ($a > 1$) is a geometrical coefficient, we must compare τ and l, and $l \neq d_0$. Note that abundance of such long pore throats produces high values of the formation factor and the specific surface area. Therefore, the proposed mechanism is in agreement with the recent experimental results of Kruschwitz *et al.* (2009).

Considering both effects at play, we combine eqs (14)–(16), substituting d for l in eq. (14), and we obtain for the surface diffusivity

$$D_s = \vartheta_s^2 \frac{l^2}{\bar{\tau}} = \vartheta_s^2 a^2 \frac{d^2}{\bar{\tau}}. \tag{17}$$

The $\vartheta_s^2 a^2$ factor determines the difference between D_{eff} obtained from eq. (14) and D_s.

To estimate the surface tortuosity of clay minerals, we used the model proposed by Moldrup *et al.* (2001), which describes diffusion in soils. Their model predicts a strong increase of the tortuosity with the decrease of the water content. We assumed that, with low water content, the tortuosity is largely influenced by the mineral surface and, therefore, the tortuosity at the low water content may be considered as the minimum estimated surface tortuosity. For clay with low water content, the model predicts the tortuosity value larger than four. Considering this value as the minimum value of the surface tortuosity, we obtain the effective diffusivity value 16 times lower than that of the surface diffusivity (eq. 15).

To explain the difference of two orders in magnitude between the surface diffusivity and the effective diffusivity, we must assume that the length of a pore throat is 2.5 times greater than its diameter. We do not have micrographs of our sandstones, but in microphotographs of Permo-Triassic sandstones from the United Kingdom (Scott & Barker 2005) such 'long' pores (and even longer ones) are observed.

Therefore, each of the above mechanisms, as well as combination thereof, allow explanation of the low values of the effective diffusivity obtained from the IP data.

5 CONCLUSIONS

In this paper, on the basis of TD measurements of six sandstone samples, we obtained RTDs. In our analysis, we used the characteristic relaxation time, which is the geometrical mean value of the modal relaxation times obtained by measuring a sample saturated with water of different electrical conductivities. We found a logarithmic correlation between d_0 and $\bar{\tau}$($R^2 = 0.95$). This logarithmic correlation is not in accordance with the existing theories, which predict the power-law relationship, eq. (13), between the grain size (or the pore throat size) and the relaxation time.

To interpret our data, we assumed that the effective ion diffusivity depends on the pore throat size. We calculated the effective diffusivity from the IP and MICP data, and we found a positive power-law relationship between the diffusivity and the pore throat diameter. The value obtained for the power-law exponent is in good agreement with the value reported by Kruschwitz *et al.* (2009). This agreement is remarkable especially because the approaches used in our paper, and those used by Kruschwitz and her co-workers are very different: we used TD measurements, and they used FD measurements; we applied the SNP model, and they used the Cole–Cole resistivity model.

For clayey samples, the calculated effective diffusivity values were found to be one to two orders in magnitude lower than those characteristic of the surface diffusion. We proposed two mechanisms to explain the low values of the effective diffusivity obtained from the IP data: the surface tortuosity effect and the pore geometry effect.

Relaxation time as a measure of the characteristic diffusion length in the pore space is not necessarily directly related to the characteristic hydraulic radii of pores. The difference between the characteristic diffusion length and the pore radius is manifested by the 'slow' diffusion, described by Kruschwitz *et al.* (2009) and confirmed and explained in this paper. This fact poses a limitation in the use of the relaxation time for predicting hydraulic conductivity values. However, we believe that in practice this obstacle may be overcome based on the combined use of the relaxation time and of the integral polarization characteristics (the normalized chargeability or the imaginary part of the complex electrical conductivity or resistivity). Because the integral parameters are sensitive to the clay content and to the specific surface area, which are probably responsible for the 'slow' diffusion, high values of these parameters should indicate and discriminate sandstones with anomalously large values of τ. For such sandstones, τ is not useful to assess k. In contrast, for clean sandstone with low polarization, τ is a useful characteristic of the hydraulic permeability.

ACKNOWLEDGMENTS

This work is partially supported by Schlumberger. K. Titov also acknowledges the support of St. Petersburg division of the Institute of Environmental Geology (Russian Academy of Sciences) and of St Petersburg State University. A. Tarasov thanks 'ElGeo' Ltd.

for the permission to use the AIE equipment for the experiments. The authors are grateful to A. Binley, to the Associated Editor J. Renner, and to an anonymous reviewer for their very constructive comments.

REFERENCES

Binley, A., Slater, L.D., Fukes, M. & Cassiani, G., 2005. Relationship between spectral induced polarization and hydraulic properties of saturated and unsaturated sandstone, *Water Res. Res.,* **41,** 1–13, doi:10.1029/2005WR004202.

Börner, F.D., Schopper, J.R. & Weller, A., 1996. Evaluation of transport and storage properties in the soil and groundwater from induced polarization measurements, *Geophys. Prospect.,* **44,** 583–601.

Brunauer, S., Emmett, P.H. & Teller, E., 1938. Adsorption of gases in multimolecular layers, *J. Am. Chem. Soc.,* **60,** 309–319, doi:10.1021/ja01269a023.

Dias, C.A., 2000, Development in a model to describe the low-frequency electrical polarization in rocks, *Geophysics,* **65,** 437–451.

Dukhin, S.S. & Shilov, V.N., 1974. *Dielectric Phenomena and the Double Layer in Disperse Systems and Polyelectrolytes,* John Wiley and Sons, New York.

Johnson, I.M., 1984. Spectral induced polarization parameters as determined through time-domain measurements, *Geophysics,* **49,** 1993–2003.

Kormiltsev, V.V., 1963. O vozbuzdenii i spade vyzvannoi polarizatsii v kapillarnoi srede (On excitation and decay of Induced Polarization in capillary medium), *Izvestia AN SSSR, Seria Geofizicheskaya* (Solid Earth Physics), **11,** 1658–1666 (in Russian).

Kruschwitz, S., Binley, A., Lesmes, D. & Elshenawy, A., 2009. Physical controls on low frequency electrical spectra of porous media, *Geophysics*, in press.

Lesmes, D.P. & Frye, K.M., 2001. Influence of pore fluid chemistry on the complex conductivity and induced polarization responses of Berea sandstones, *J. geophys. Res.,* **106,** 4079–4090.

Lesmes, D.P. & Morgan, F.D., 2001. Dielectric spectroscopy of sedimentary rocks, *J. geophys. Res.,* **106,** 13 329–13 346.

Lewis, R.J.G., 1985. The determination of spectral parameters with pulse-train induced polarization, *Geophysics,* **50,** 870–871.

Marshall, D.J. & Madden, T.K., 1959. Induced polarization, a study of its causes, *Geophysics,* **24,** 790–816.

Martil, R., Delgado, A., La Iglesia, A. & Ramseyer, K., 2003. Origin and diagenetic evalution of kaolin in reservoir sandstones and associated shales of the Jurassic and Cretaceous Salam field western desert (Egypt), in *Clay Mineral Cement in Sandstones,* pp. 319–342, eds Worden, R.H., & Morad, S., Special Publication of the Int. Ass. Sedimentologists, Blackwell Publishing, Oxford.

Moldrup, P., Olsen, T., Komatsu, T., Schjonning, P. & Rolston, D.E., 2001. Tortuosity, diffusivity, and permeability in the soil liquid and gaseous phases. *Soil. Sci. Soc. Am. J.,* **65,** 613–623.

Morgan, F.D. & Lesmes, D.P., 1994. Inversion for dielectric relaxation spectra, *J. Chem. Phys.,* **100,** 671–681.

Pelton, W.H. Ward S.H., Hallof, P.G., Sill, W.R. & Nelson, P.H., 1978. Mineral discrimination and removal of inductive coupling with multifrequency IP, *Geophysics,* **43,** 588–609.

Pelton, W.H., Sill, W.R. & Smith, B.D., 1983. Interpretation of complex resistivity and dielectric data. Part 1, *Geophys. Trans.,* **29**(3), 297–330.

Purcell, W.R., 1949. Capillary pressure – their measurements using mercury and the calculation of permeability therefrom, *AIME Petrol. Trans.,* **186,** 39–48.

Revil, A., 1999. Ionic diffusivity, electrical conductivity, membrane and thermoelectric potentials in colloid and granular porous media: a unified model, *J. Coll. Interface Sci.,* **212,** 503–522.

Schwarz, G., 1962. A theory of the low-frequency dispersion of colloidal particles in electrolyte solution, *J. Phys. Chem.,* **66,** 2636–2642.

Scott, J.B.T., 2004. Low-Frequency electrical spectroscopy of sandstone, *Unpublished PhD thesis*. School of Geography, Earth and Environmental Sciences. The University of Birmingham.

Scott, J.B.T. & Barker, R.D., 2003. Determining pore-throat size in Permo-Triassic sandstones from low-frequency electrical spectroscopy, *Geophys. Res. Lett.,* **30**(9), 1450, doi:10.1029/2003GL016951.

Scott, J.B.T. & Barker, R.D., 2005. Characterization of sandstone by electrical spectroscopy for stratigraphical and hydrogeological investigations, *Quart. J. Eng. Geol. Hydrogeol.,* **38,** 143–154.

Soininen, H., 1984. Inapplicability of pulse train time-domain measurements to spectral induced polarization, *Geophysics,* **49,** 826–827.

Soxhlet, F., 1879. Die gewichtsanalytische Bestimmung des Milchfettes, *Polytechnisches J. (Dingler's)*, **232,** 461.

Tarasov, A., 2008. Induced polarization relaxation time distribution of ion-conductive rocks. *Unpublished PhD thesis*. St. Petersburg State University, 120 pp.

Tarasov, A., & Titov, K., 2007. Relaxation time distribution from time domain induced polarization measurements, *Geophys. J. Int.,* **170,** 31–43.

Tarasov, A., Titov, K., Münch, M. & Kemna, A., 2003. Induced polarization spectra of sands and clays measured in the time domain, *Proceedings of the International Geophysical Conference and Exhibition at Moscow. "Geophysics of 21 Century: The Leap into the Future",* Moscow, 6–10 September 2003, PS11, P6 (CD).

Tikhonov, A.N. & Arsenin, V.Ya., 1986. *Metody Reshenia Nekorrektnykh Zadach* (Methods for solving ill posed problems), Nauka, Moscow (in Russian).

Titov, K., Komarov, V., Tarasov, V. & Levitski, A., 2002. Theoretical and experimental study of time-domain induced polarization in water saturated sands, *J. appl. Geophys.,* **50,** 417–433.

Titov, K., Kemna, A., Tarasov, A. & Vereecken, H., 2004. Induced polarization of unsaturated sands determined through time-domain measurements. *Vadose Zone J.,* **3,** 1160–1168.

Tong, M., Li, L., Wang, W. & Jiang, Y., 2006. Determining capillary pressure curve, pore-seze distribution and permeability from induced polarization of shaley sand, *Geophysics,* **71,** 33–40.